2017 IEEE International Conference on Robotics and Automation (ICRA)
Singapore, May 29 - June 3, 2017

Roboscope: A Flexible and Bendable Surgical Robot for Single Portal Minimally Invasive Surgery

Jacob Rosen[1], Laligam N. Sekhar[2], Daniel Glozman[3], Muneaki Miyasaka[4], Jesse Dosher[5], Brian Dellon[6]
Kris S. Moe[7], Aylin Kim[8], Louis J. Kim[2], Thomas Lendvay[9], Yangming Li[4], Blake Hannaford[4]

***Abstract*— Minimally Invasive Surgery (MIS) can reduce iatrogenic injury and decrease the possibility of surgical complications. This paper presents a novel flexible and bendable endoscopic device, "Roboscope", which delivers two instruments, two miniature scanning fiber endoscopes, and a suction/irrigation port to the operation site through a single portal. Compared with existing bendable and steerable robotic surgical systems, Roboscope provides two bending degrees of freedom for its outer sheath and two insertion degrees of freedom, while simultaneously delivering two instruments and two endoscopes to the surgical site. Each bending axis and insertion freedom of Roboscope is independently controllable via an external actuation pack. Surgical tools can be changed without retracting the robot arm. This paper presents the design of the Roboscope mechanical system, electrical system, and control and software systems, design requirements and prototyping validation as well as analysis of Roboscope workspece.**

***Index Terms*— Surgical Robot, Flexible and Bendable Robot, System Design, Skullbase and Sinus Surgery, NeuroSurgery**

I. Introduction

The development of Minimally Invasive Surgery (MIS) techniques has greatly decreased surgical morbidity and post-operative recovery time, and therefore gains more clinical interests. At the same time, these techniques have created new challenges and changed the skills required of surgeons; where open-field surgery allowed wide visualization of anatomy, endoscopic procedures lose this perspective and require operating in tight confines bordered by critical structures that are only partially visible [1]. Various surgical instruments and surgical robots have been developed to facilitate MISs.

The widely available surgical robot platforms, such as da Vinci, accesses pathology through elongated, steerable instrument, such as the EndoWrist series instruments [2], [3]. These robots not only provide improved degree of freedom of movement, but also magnified 3D endoscopic view and reduced hand tremor.

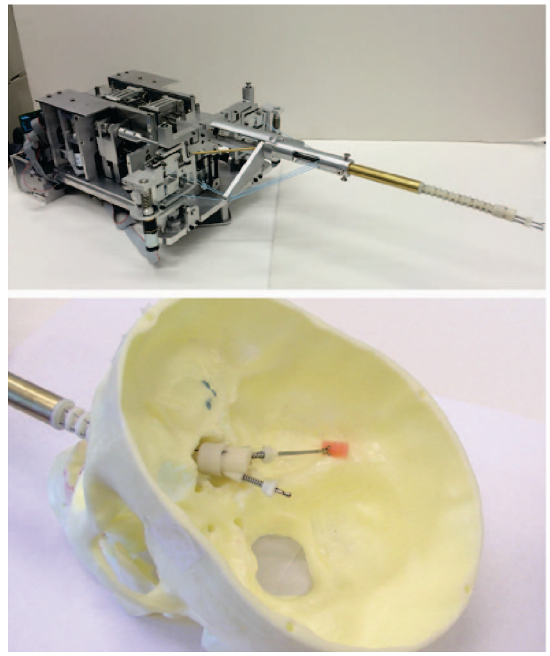

Fig. 1. Top: Roboscope. A surgical robot for single portal minimally invasive surgery. Bottom: Example of use. Roboscope reached to the very deep site of skull baseand and fetched the target object through nose without bone cutting.

Although these straight-line instruments are very useful for many surgeries, for other surgeries in highly confined spaces and more difficult to access, such as neurosurgery, flexible and bendable surgical robots are desired. Concentric-tube robots can work dexterously in narrow, constrained, and winding spaces and have attracted much research interest [5], [6], [7]. However, concentric tube robots are not able to deliver multiple instruments, such as gripper or scissors to the pathology. The surgical robots developed by Clark et al. [8] and Seneci et al. [9] adopted larger tubes able to deliver a single instrument via curved pathways. Lee et al. [10] developed a two-arm 30 mm diameter flexible robot which can deliver two types of instruments to the pathology through a single portal with stereo visualization, high precision and dexterity. But the surgical instruments mounted on this robot are not easy to exchange and the sterilization of the robot remains a challenging problem so far.

In this paper, we introduce a novel flexible and bendable surgical robot, the Roboscope Surgical System (Fig. 1), which is designed to provide full functionality for skullbase

[1]Bionics Lab, Department of Mechanical and Aerospace Engineering, University of California, Los Angeles, Los Angeles, CA, USA 90095
[2]Department of Neurological Surgery, University of Washington, Seattle, WA, USA 98195
[3]Magenta Medical Ltd., Israel
[4]BioRobotics Lab., Department of Electrical Engineering, University of Washington, Seattle, WA, USA 98195
[5]Applied Physics Laboratory, University of Washington, Seattle, WA, USA 98195
[6]Department of Computer Science and Engineering, University of Washington, Seattle, WA, USA 98195
[7]Department of Otolaryngology Head and Neck Surgery, University of Washington, Seattle, WA, USA 98195
[8]SPI Surgical Inc., Seattle, WA, USA 98199
[9]Department of Urology, University of Washington, Seattle, WA, USA 98195

surgeries and neurosurgery. Comparing with existing bendable and steerable robotic surgical systems:

- Roboscope provides highly dexterous motion (12 mechanical Degrees of Freedom (DOFs)) along the following axes:
  - bending of the main shaft in two directions (2 DOFs)
  - independent 2-way deflection of two inserted instruments ($2 \times 2 = 4$ DOFs)
  - insertion/withdrawal motion of each of the two inserted instruments ($1 \times 2 = 2$ DOFs)
  - axial rotation of the instruments ($1 \times 2 = 2$ DOFs)
  - jaw actuation of the instruments ($1 \times 2 = 2$ DOFs)
- Roboscope provides 3-dimensional endoscopic vision through two, 1.2 mm, channels able to house Scanning Fiber Endoscopes [11], [12].
- Roboscope provides instruments and visualization in approximate correspondence with human hand and eye spatial relationships (Fig. 2).

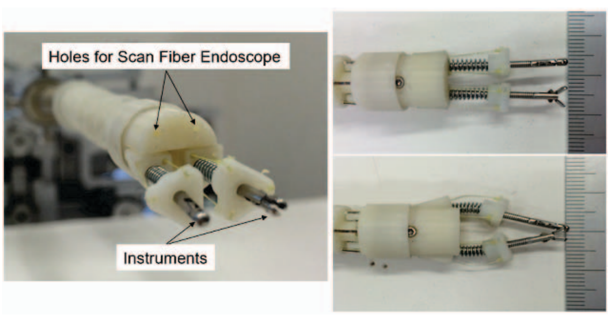

Fig. 2. Roboscope Tip. Roboscope provides instruments and visualization in approximate correspondence with human hand and eye spatial relationships. The diameter of the instruments in the image is 2 mm.

- Roboscope supports interchange of surgical instruments without removal of the system from the patient.

The contribution of this paper includes:

- We introduce Roboscope, a novel flexible and bendable surgical robot, for the first time;
- We specify the design requirements for the flexible surgical robot that is applicable to skull base and sinus surgeries, and neurosurgery, through analysis of surgical motion data and discussion with surgeons;
- We initially validate the functionality of Roboscope through cadaver experiment;
- We describe the mechanical design, electrical design and software design for Roboscope;
- We analyze the workspace of the flexible joints;

The paper is organized as follows. Section II introduces the design requirements; Section III describes the prototype verification of Roboscope; Section IV introduces the design details of Roboscope, including mechanical design, electrical design and software system design; Section V presents the workspace covered by the flexible joints of the Roboscope. Conclusions are drawn in Section VI.

II. Design Requirements

The Roboscope Surgical System (RSS) is designed to leverage an innovative new endoscopic imaging technology [11], [12] and to improve the quality and cost-effectiveness of surgical care. The task requirements for Roboscope are the ability to perform surgery on a smaller scale (microsurgery), and access to small curved corridors through natural orifices (minimally invasive surgery), the ability for telesurgery, and reducing the surgeons physiological tremor 10-fold [13], [14].

A. Design Requirement for Minimally Invasive Skullbase and Sinus Robots

Instrument motions from experienced surgeons were collected at 10Hz by Stryker iNtellect systems on a cadaver to specify the design requirements for surgical robot working in Skullbase and Sinus areas [15]. Four annotation points implanted into the cadaver were used to align CT scans with the cadaver. Both the tip of the instrument and the center of the tracking device are recorded. Therefore, positions, linear velocity and acceleration can be retrieved from the data, as listed in Table. I and shown in Fig. 3. These data are important for motor and gear ratio selection in the system design.

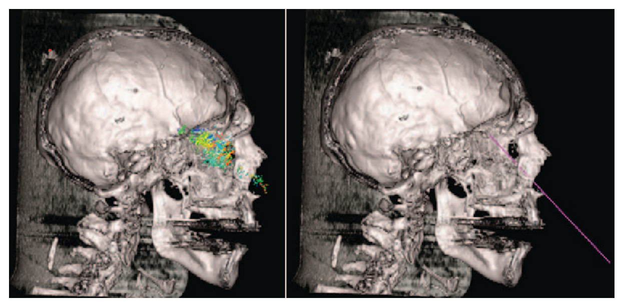

Fig. 3. Motion Data Collected for Roboscope Design Specification. Colored points in the left figure are tip positions recorded by the Stryker iNtellect system, the purple line in the right figure indicated instrument pose during a surgery.

In order to provide full neurosurgery functionality, Roboscope also needs to deliver various instruments to the pathology as well as provide high quality endoscopic visualization of the surgical site.

III. Prototype Verification

An initial prototype manipulation system was quickly developed (Fig. 4). The initial Roboscope prototype consisted of a 14 mm diameter main shaft, which delivered two, 2.3 mm diameter, tool shafts and two 1.2 mm scanning fiber endoscopes to the surgical site; the main shaft provided two directions of bending.

The two instruments were introduced through full length continuous lumens to deflection collars mounted on springs and deflectable in two directions by remote cable drives. The two instruments were commercial manually operated urological forceps and scissors (blue handles, Fig 4) placed through channels which enable exchanging instruments without retracting the whole robot.

Roboscope visualization is provided by either one or two fiber optic 1.2 mm flexible endoscopes developed by Prof. Eric Seibel of the University of Washington. The scanning

TABLE I

SKULLBASE AND SINUS SURGICAL MOTION DATA FROM EXPERT SURGEONS.

	Max	Min	Averaged	SD	95%Value
Velocity(mm/s)	199.99876	0.02626	21.13201	27.03502	76.50937
Acceleration(mm/s^2)	1758.98390	0.42714	173.49796	315.41424	506.16889

fiber endoscope (SFE) provides high-quality, wide-field, full-color laser based video imaging in a 1.2 mm flexible fiber [11], [17]. The SFE includes its own illumination and two can be configured for stereo visualization. Roboscope contains channels for two SFEs but only one was available for testing.

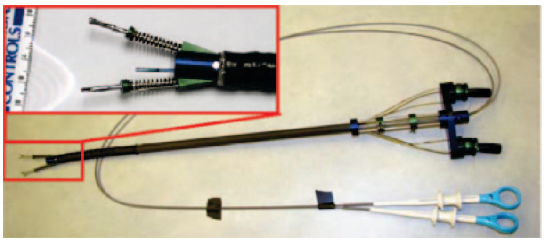

Fig. 4. Prototype for Design Verification. Manual control is required for prototype operation. Inset shows two instruments in their deflectors and the SFE (between instruments). Note light cone emitted from the SFE intersecting tabletop.

We first validated the design on cadaver tests (Fig. 5), operated with joysticks (Fig. 4). The system was inserted into a cadaver head, and the pituitary fossa was visualized by the SFE (Fig. 5, Right), the right hand tool was manipulated in a coordinated manner, including tool opening, rotation and extension so that it grasped a portion of the pituitary gland; and a bit of the tissue was successfully excised by surgeons. Range of motion was measured for the prototype in each of its motion directions. Results are summarized in Table II.

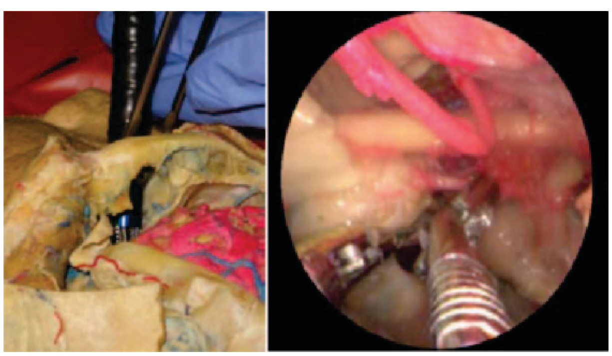

Fig. 5. Prototype Validation in Cadaver. Roboscope Arm inserted into the orbit and visible through dissection looking from above the supraorbital arch (Left). Image captured from fiber endoscope during tissue manipulation (Right). Scale: instrument shaft at 6 O'clock has a diameter of 2.3 mm.

TABLE II

PROTOTYPE RANGE OF MOTION.

Axis	Positive Motion	Negative Motion
Bending Section (up/down)	180°	140°
Bending Section (left/right)	140°	140°
Tool Steering (all directions)	50°	50°

IV. ROBOSCOPE SYSTEM DESCRIPTION

A. Mechanical Design

The Roboscope system is composed of the tool assembly and five major assemblies, including the Base, Linear Control Actuator (LCA), two 2-DOF Tool Motion Boxes (TMB), gimbal, and the Electrical assembly.

1) Tool Assembly: The tool assembly consists of the elongated shaft and interchangeable flexible endoscopic tool systems (Fig. 6). The flexible joint is designed based on the range of motion in Table. II. The tool assembly houses the two instruments and the two endoscopes. While complete sterile barrier has not yet been achieved in this design, the tool assembly is designed for sterilization and isolates surgical instruments and endoscopes from the drive system. The main directional joint is driven by the two drive blocks (green cubes, Fig. 6) and provides gross pitch and yaw positioning for the Roboscope; These motions of the main directional joint are made possible by cables running from the drive blocks to the directional joint. The main directional joint consists of serially connected multiple bending segments (Fig. 7). Each bending segment has holes for all actuation cables, instruments, and scanning fiber endoscopes to go through. This avoids high friction and wear that could be caused by tangling and inter sliding of cables and instruments especially while the joint is being bent. In a second prototype, the main shaft and directional joint had a diameter of 8 mm in order to fit natural orifice trans-nasal and trans-orbital surgeries. Currently, for a quick verification of the system, the parts were 3D printed with ABS plastic and the diameter was increased to 12 mm in order to avoid failure during manipulation. However, dimension-wise (considering the size of the instruments and scan fiber endoscope), it is still possible to achieve 8 mm diameter. Two tool direction joints and two endoscope ports are located at the end of the main directional joint; and each of the tool directional joints are driven by three cables separated by 120 degrees, in order to provide pitch and yaw control.

2) Gimbal Assembly: The gimbal assembly is used to control the tool directional joint (Fig. 8). Unlike the linear drive blocks of the main joint, the tool joints are controlled by three cables (D) separated at the swashplate (A) by 120 degrees instead of four cables at 90 degrees. The gimbal twisters (B) rotate the swashplate in two orthogonal directions through the center of a circle made by the three cable attachment points. The gimbal assembly is interfaced with the tool assembly through holes and slots (C), therefore, the tool assembly that meets the sterilization requirements can be easily detached from the base.

3) Linear Control Actuator: The Linear Control Actuator assembly actuates the main directional joint (Fig. 9). Lead

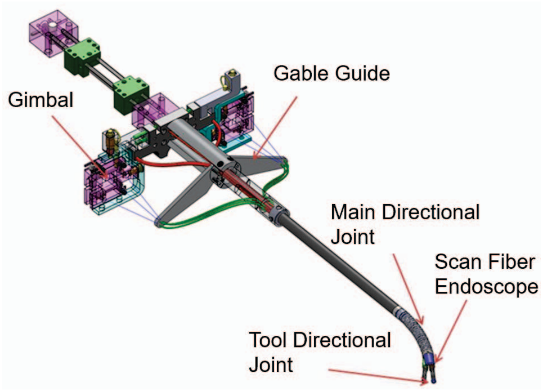

Fig. 6. Tool assembly: a sterilizable unit which will allow sterile tools to be exchanged without retracting the full arm. A complete sterile barrier has not yet been designed.

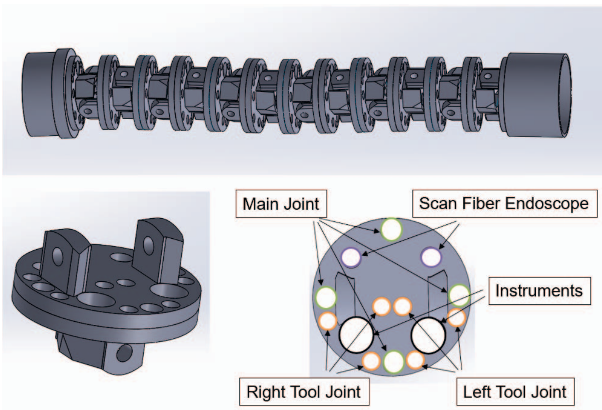

Fig. 7. Top: Main directional joint. Bottom Left: One bending segment of main directional joint. Bottom Right: Top view of a bending segment. Each segment has holes for all actuation cables, instruments, and scan fiber endoscopes to avoid unpredictable friction caused by tangling and inter wire sliding.

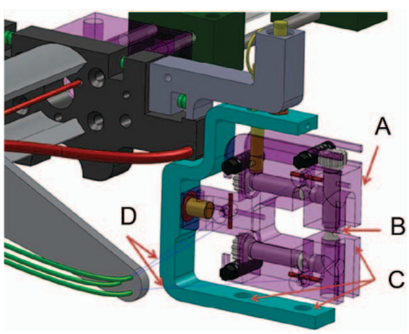

Fig. 8. Gimbal assembly. The unit is used to control the tool directional joint.

screws (A) are turned to move the drive blocks (the two green parts) by timing belt (G). The block carriages (B) ride along high precision, low friction rails (C) to ensure smooth and straight travel and to act against the moment created by the screw. The tool assembly is aligned with the linear control actuator assembly by Locating pins (D) and is locked by the locking lids (E). The lids may easily be opened through an integrated spring-loaded plunger (F) for Roboscope removal. Motors are indicated as H.

4) Tool Motion Box: The tool motion box houses the motors used for driving instruments (Fig. 10). The main

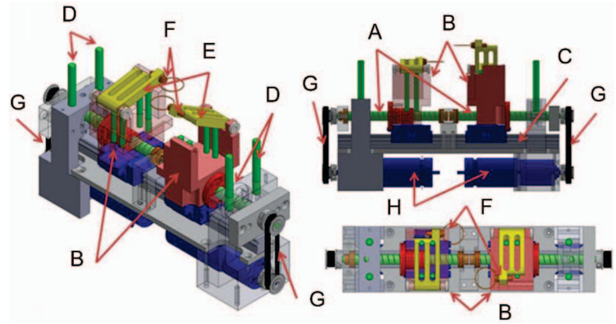

Fig. 9. Linear Control Actuator. It provides motion control for the main directional joint.

challenge for tool motion box design is to maintain the ability to indefinitely twist the instrument while actuating the instruments open-close axis at the same time. Actuation of the instrument is accomplished by moving an inner cable in or out with respect to its outer housing, therefore, the inner cable is attached to collar (E) while the outer housing is clamped to collar (C). In order to keep the worm gear in the correct location, a spring (G) is loaded between the gear and a thrust bearing (F) to counteract the linear frictional forces created by the extension/retraction of the tool. The insertion/withdraw axis is driven by a lead-screw (B) and Motor (A).

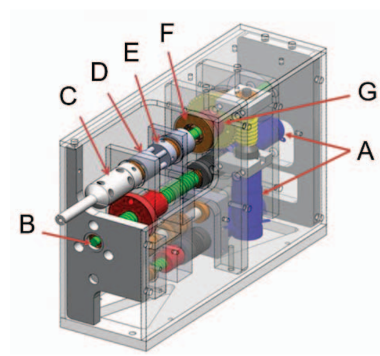

Fig. 10. Tool Motion Box maintains the ability to indefinitely twist instruments, while the instrument was actuating at the same time.

5) Electrical Assembly: The compact design of the Roboscope makes the cable routing and hookup a challenging problem (Fig. 11). The base (A) was skeletonized to allow dropping cables to the bottom layer (B); therefore, all wires can be easily routed to the back of the actuator pack, to connect with the printed circuit boards (D), which is connected to large power and signal trunk cables (C). The electrical assembly is connected to the external electronics through connectors (E) mounted to absorb the external forces and protect the PCBs.

6) Base: The base is a skeletonized aluminum structure which handles cable routing and serves as a robust platform for the other assemblies (Fig. 12). The complete actuation pack assembly is shown in Fig. 12. Two tool motion boxes (B) are located on the top of the base (E), and are by the side of the Linear Control Actuator (D); while the electrical assembly (F) is located at the rear of the actuation pack. The gimbal assembly (C) is in front of the base and extra

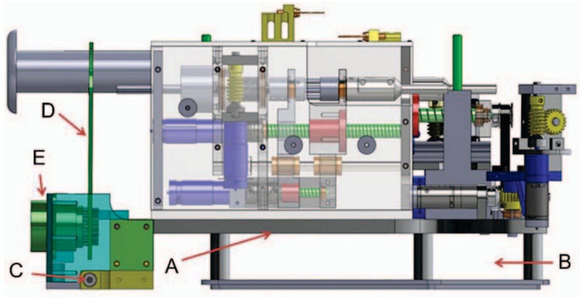

Fig. 11. Electrical assembly. It connects the Roboscope with the Raven Power Box and protects electronics in the Roboscope.

tools/cameras are inserted through channels (A).

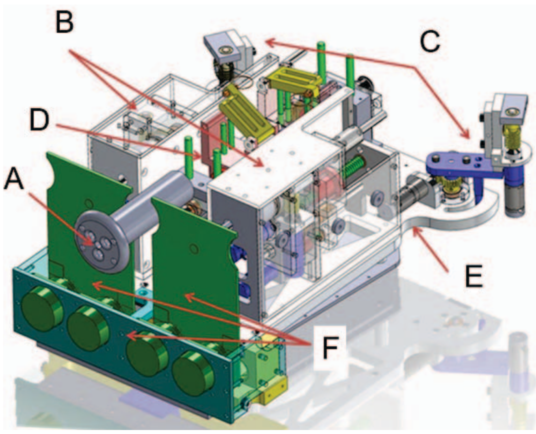

Fig. 12. Relative Position Among Base and Other Assemblies. Base supports and connect other assemblies.

B. Electrical Design

1) Electronics and Driver: The Roboscope uses the same electronics and drivers as the Raven II robotic system[3]. Two amplifier control boxes operate up to 8 motors each and communicate with a computer via USB. A power box contains power supplies and a programmable logic controller (PLC) which performs safety oversight of the system including watchdog timer and emergency stop. The software drivers for each motion axis were implemented on the Linux real-time patch kernel and is available here [18].

2) Motors: Motors and gear heads are selected to meet the velocity and acceleration requirement mentioned in Section II-A. Four types of brushed motors and four types of gear heads are adopted in the Roboscope. The most powerful 9 Watt motors are used for driving the main directional joints; 1.2 Watt motors are selected for driving tool directional joints. Two different 2.5 Watt motors were selected for the Tool Motion Box, with the difference that the motor/gear-head combination for instrument open-close control generates very slow movement.

C. Control System and Software

The Roboscope software architecture (Fig. 13) is based on the open and extendable software architecture for the Raven surgical robotics platform, now in use at 18 universities[3], [4]. Four principal layers comprise this system: Linux, configured for deterministic real-time scheduling, a 1000Hz control process which handles coordinate transformations, kinematics, control, gravity compensation and similar functions, ROS[19], a widely used open- source middleware layer, and the application layer. We use an existing user-datagram-protocol (UDP) based interoperable teleoperation protocol (ITP)[20] which will be adapted to connect the Roboscope to a user interface.

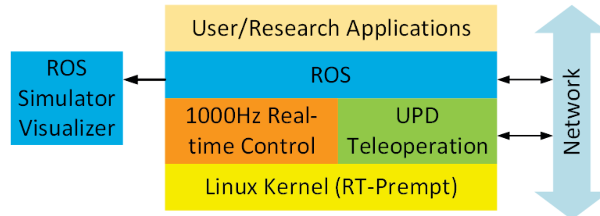

Fig. 13. Software Architecture. The software architecture is shared by the Roboscope and the Raven II robot.

V. Workspace

The workspace of the main directional joint and tool directional joint (left and right) is calculated individually based kinematic analysis. The base frame of each joint and notations of the left and right tool location are assigned as shown in Fig. 14.

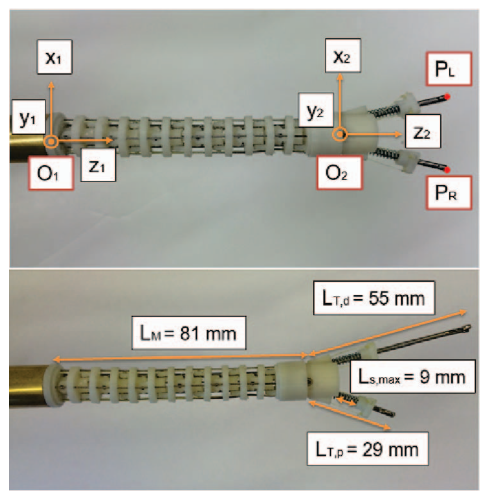

Fig. 14. Top view of the flexible joint. Top: Frame assignments for the joints. z_1 and z_2 are along the center of the main directional joint. Bottom: Lengths of the main directional joint (L_M), tool directional joint (at its proximal limit ($L_{T,p}$) and distal limit ($L_{T,d}$)), and spring in the tool directional joint at its natural or maximum length ($L_{s,max}$).

A. Main Directional Joint

The main directional joint consists of 12 segments; 6 segments rotate about the x-axis and the other 6 rotate about the y-axis. x and y rotation segments are connected alternately and all segments have a range of motion of ± 30 degrees. It is assumed that all segments for each x and y rotation rotate equally and have a constant curvature. Using Denavit-Hartenberg (DH) convention, the kinematics is obtained and the result is shown in Fig. 15. Fig. 16 shows the shapes of the main directional joint when it is at $P_{M,1}$, $P_{M,2}$, and $P_{M,3}$.

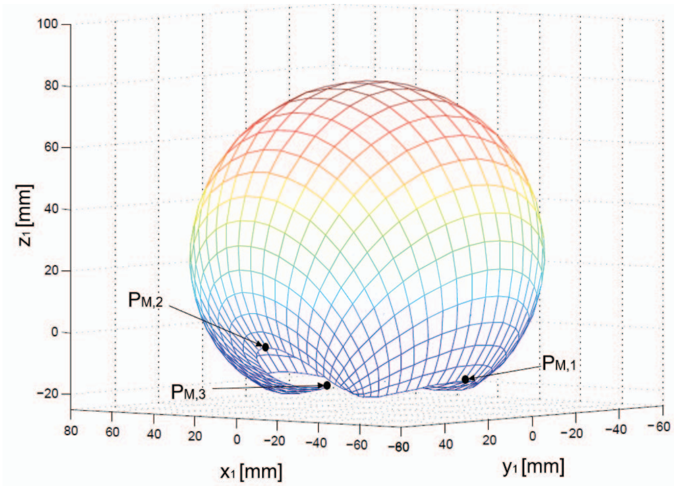

Fig. 15. Simulation of 2D manifold workspace for the main directional joint. Position of O_2 with respect to O_1.

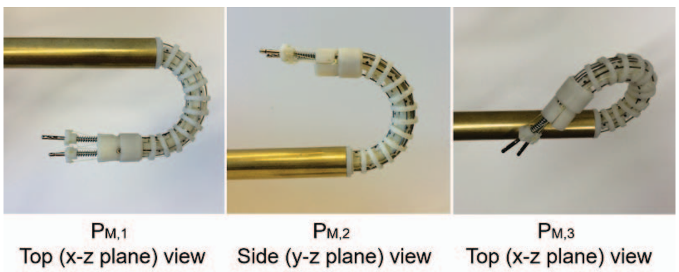

Fig. 16. Shapes of the main directional joint when the positions are $P_{M,1}$ (left), $P_{M,2}$ (middle), and $P_{M,3}$ (right).

B. Tool Directional Joint

The kinematic model of the tool directional joint was developed using the angle-curvature approach presented in [23] with assumptions for the helical spring described in [24]. Since the amount the actuation cables are pulled (δl_i ($i = 1,2,3$)) is controlled by the motion of the gimbal and swash plate, δl_i is written as a function of gimbal angles θ_x and θ_y.

$$\delta l_i = |\overline{G_iP_i}| - |\overline{G_{i,0}P_i}| \tag{1}$$

$$\overline{G_iP_i} = -R_G G_i + P_i \tag{2}$$

$$\overline{G_{i,0}P_i} = -G_{i,0} + P_i \tag{3}$$

$$R_G = R_y(\theta_y)R_x(\theta_x) \tag{4}$$

where G_i is the point cable is fixed on the gimbal, $G_{i,0}$ is the position of G_i when $\theta_x = \theta_y = 0$, P_i is the cable guide point on the tool assembly (Fig. 6, 17), and R_x and R_y are the rotational matrices. The result is shown in Fig. 18. Pictures of the tool directional joint when the position is $P_{T,1}$, $P_{T,2}$, and $P_{T,3}$ are shown in Fig. 19.

The angles of the main directional joint at $P_{M,1}$, $P_{M,2}$, $P_{M,3}$ and tool directional joint at $P_{T,1}$, $P_{T,2}$, $P_{T,3}$ were measured using a protractor. Calculated and measured angles are summarized in Table III.

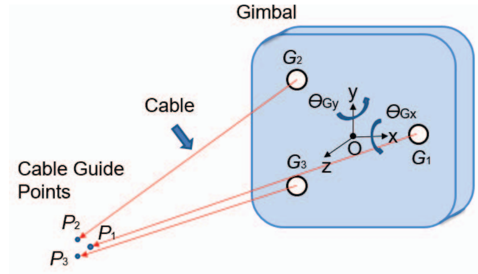

Fig. 17. Schematic drawing of the gimbal and the cable guide points. Cable length $|\overline{G_iP_i}|$ changes as the gimbal rotates about its x and y axes.

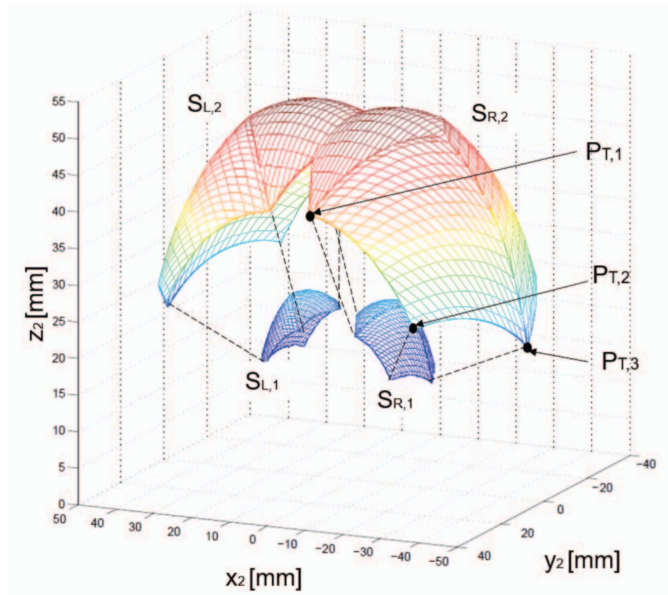

Fig. 18. Simulation of workspace for the tool directional joint. Positions of the left tool P_L and right tool P_R are with respect to O_2. $S_{L,1}$ and $S_{R,1}$ show the workspace when the tools are at the proximal limit and $S_{L,2}$ and $S_{R,2}$ show the workspace when the tools are at the distal limit. The whole workspace of each tool is the space covered by linear projection of inner to outer surface. (i.e. $S_{L,1}$ to $S_{L,2}$ for the left tool and $S_{R,1}$ to $S_{R,2}$ for the right tool).

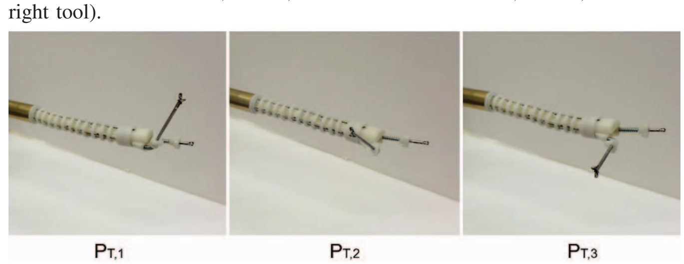

Fig. 19. Shapes of the tool directional joint when the positions are $P_{T,1}$ (left), $P_{T,2}$ (middle), and $P_{T,3}$ (right).

VI. Conclusion

The roboscope achieved a new level of dexterity (12 mechanical DOFs) and situational awareness (via the two scanning fiber endoscopes (including illumination) in flexible shaft diameter as low as 8 mm. The Roboscope was designed and developed to further decrease iatrogenic injury in minimally invasive neurosurgery through delivery of two instruments, two endoscopes, and a suction/irrigation port to the operation site through a single portal.

TABLE III

ROBOSCOPE JOINT BENDABLE ANGLE.

	Position	Angle	
		Calculated	Measured
Main Directional Joint	$P_{M,1}$	180°	180°
	$P_{M,2}$	256°	251°
	$P_{M,3}$	180°	180°
Tool Directional Joint	$P_{T,1}$	51.7°	52°
	$P_{T,2}$	51.3°	51°
	$P_{T,3}$	51.7°	50°

The Roboscope mechanical design successfully isolated the tools and the endoscopes from any actuators and makes possible the exchange of tools. The electrical design utilized previous results from the Raven II robot in order to enforce instrument safety. The software was designed to have both robustness, which is critical to surgical applications, and extensibility, which helps researchers to use the robot.

Further work on Roboscope will include teleoperated cadaver studies, development of a sterile barrier, and integration of recent results on control of cable driven mechanisms [21] within the Roboscope control and modeling of the cable within a segmented bending section [22].

The workspace for the main and tool directional joint is obtained individually. Since there are effects of coupling, the presented workspace for the tool directional joint is correct only when the main directional joint is straight. When the main directional joint is bent, the tool directional joint's workspace deviates from the one presented. Therefore, further investigation needs to be performed to fully understand the inter relation of the joints.

ACKNOWLEDGMENT

This work is supported by Department of Defense STTR Phase II Grant W81XWH-09-C-0159, NSF grant CPS-0930930 and award IIS-1227184: Multilateral Manipulation by Human-Robot, and NIH grant 5R21EB016122-02. The authors would like to thank to the members of Biorobotics lab, University of Washington and SPI Surgical Inc. for their support and contribution throughout the entire project.

REFERENCES

[1] D. Nuss, R. E. Kelly, D. P. Croitoru, and M. E. Katz, "A 10-year review of a minimally invasive technique for the correction of pectus excavatum," *Journal of pediatric surgery*, vol. 33, no. 4, pp. 545–552, 1998.

[2] https://www.intuitivesurgical.com.

[3] B. Hannaford, J. Rosen, D. W. Friedman, H. King, P. Roan, L. Cheng, D. Glozman, J. Ma, S. N. Kosari, and L. White, "Raven-ii: an open platform for surgical robotics research," *Biomedical Engineering, IEEE Transactions on*, vol. 60, no. 4, pp. 954–959, 2013.

[4] https://github.com/uw-biorobotics/raven2.

[5] P. E. Dupont, J. Lock, B. Itkowitz, and E. Butler, "Design and control of concentric-tube robots," *Robotics, IEEE Transactions on*, vol. 26, no. 2, pp. 209–225, 2010.

[6] D. C. Rucker, R. J. Webster, G. S. Chirikjian, and N. J. Cowan, "Equilibrium conformations of concentric-tube continuum robots," *The International journal of robotics research*, 2010.

[7] P. J. Swaney, H. B. Gilbert, R. J. Webster, P. T. Russell, K. D. Weaver, "Endonasal skull base tumor removal using concentric tube continuum robots: a phantom study," *J Neurol Surg B Skull Base*, 2014.

[8] J. Clark, D. P. Noonan, V. Vitiello, M. H. Sodergren, J. Shang, C. J. Payne, T. P. Cundy, G.-Z. Yang, and A. Darzi, "A novel flexible hyper-redundant surgical robot: prototype evaluation using a single incision flexible access pelvic application as a clinical exemplar," *Surgical endoscopy*, vol. 29, no. 3, pp. 658–667, 2014.

[9] C. Seneci, J. Shang, K. Leibrandt, V. Vitiello, N. Patel, A. Darzi, J. Teare, G.-Z. Yang *et al.*, "Design and evaluation of a novel flexible robot for transluminal and endoluminal surgery," in *Intelligent Robots and Systems (IROS 2014), 2014 IEEE/RSJ International Conference on*. IEEE, 2014, pp. 1314–1321.

[10] J. Lee, J. Kim, K.-K. Lee, S. Hyung, Y.-J. Kim, W. Kwon, K. Roh, and J.-Y. Choi, "Modeling and control of robotic surgical platform for single-port access surgery," in *Intelligent Robots and Systems (IROS 2014), 2014 IEEE/RSJ International Conference on*. IEEE, 2014, pp. 3489–3495.

[11] C. M. Lee, C. J. Engelbrecht, T. D. Soper, F. Helmchen, and E. J. Seibel, "Scanning fiber endoscopy with highly flexible, 1 mm catheterscopes for wide-field, full-color imaging," *Journal of biophotonics*, vol. 3, no. 5-6, pp. 385–407, 2010.

[12] E. J. Seibel, R. S. Johnston, and C. D. Melville, "A full-color scanning fiber endoscope," in *Biomedical Optics 2006*. International Society for Optics and Photonics, 2006, pp. 608 303–608 303.

[13] N. Nathoo, M. C. Çavusoglu, M. A. Vogelbaum, and G. H. Barnett, "In touch with robotics: neurosurgery for the future," *Neurosurgery*, vol. 56, no. 3, pp. 421–433, 2005.

[14] P. B. McBeth, D. F. Louw, P. R. Rizun, and G. R. Sutherland, "Robotics in neurosurgery," *The American Journal of Surgery*, vol. 188, no. 4, pp. 68–75, 2004.

[15] https://www.stryker.com/en-us/products/SurgicalNavigationSoftware/ENTNavigationSoftware/index.htm.

[16] C. M. Lee, C. J. Engelbrecht, T. D. Soper, F. Helmchen, and E. J. Seibel, "Scanning fiber endoscopy with highly flexible, 1 mm catheterscopes for wide-field, full-color imaging," *Journal of biophotonics*, vol. 3, no. 5-6, pp. 385–407, 2010.

[17] I. Yeoh, P. Reinhall, M. Berg, and E. Seibel, "Self-contained image recalibration in a scanning fiber endoscope using piezoelectric sensing," *Journal of Medical Devices*, vol. 9, no. 1, p. 011004, 2015.

[18] https://github.com/uw-biorobotics/usb-board-driver.

[19] M. Quigley, K. Conley, B. Gerkey, J. Faust, T. Foote, J. Leibs, R. Wheeler, and A. Y. Ng, "Ros: an open-source robot operating system," in *ICRA workshop on open source software*, vol. 3, no. 3.2, 2009, p. 5.

[20] H. King, K. Tadano, R. Donlin, D. Friedman, M. J. Lum, V. Asch, C. Wang, K. Kawashima, and B. Hannaford, "Preliminary protocol for interoperable telesurgery," in *Advanced Robotics, 2009. ICAR 2009. International Conference on*. IEEE, 2009, pp. 1–6.

[21] M. Haghighipanah, Y. Li, M. Miyasaka, and B. Hannaford. "Improving position precision of a servo-controlled elastic cable driven surgical robot using unscented kalman filter," in *Int. Conf. on Intelligent Robots and Systems (IROS)*, Hamburg, German, Oct. 2015.

[22] M. Miyasaka, M. Haghighipanah, Y. Li, and B. Hannaford. "Hysteresis model of longitudinally loaded cable for cable driven robots and identification of the parameters," in *Int. Conf. on Robotics and Automation (ICRA)*, Stockholm, Sweden, May. 2016.

[23] R. J. Webster and B. A. Jones. "Design and kinematic modeling of constant curvature continuum robots: A review," in *The International Journal of Robotics Research*, Res., vol. 29, pp.1661-1683 2010.

[24] K. Cao, R. Kang, J. Wang, Z. Song, J. Dai. "Kinematic Model and Workspace Analysis of Tendon-driven Continuum Robots," in *Proceedings of the 14th IFToMM World Congress*,pp.640-644 2015.